Robotica (2015) volume 33, pp. 1686–1703. © Cambridge University Press 2014
doi:10.1017/S0263574714000988

Kinematic analysis and workspace determination of hexarot-a novel 6-DOF parallel manipulator with a rotation-symmetric arm system

Mohammad Reza Chalak Qazani†, Siamak Pedrammehr‡,*, Arash Rahmani§, Behzad Danaei§, Mir Mohammad Ettefagh§, Aslan Khani Sheikh Rajab¶ and Hamid Abdi‖

†*Faculty of Technology & Engineering, Department of Mechanical Engineering, Tarbiat Modares University, Tehran, Iran*
‡ *Faculty of Engineering and Natural Sciences, Sabanci University, Tuzla, Istanbul, Turkey*
§*Faculty of Mechanical Engineering, University of Tabriz, Tabriz, Iran*
¶*Department of Mechanical Engineering, Ilkhchi Branch, Islamic Azad University, Ilkhchi, Iran*
‖*Centre for Intelligent Systems Research, Deakin University, Waurn Ponds Campus, Victoria 3217, Australia*

(Accepted March 19, 2014. First published online: April 29, 2014)

SUMMARY
Parallel mechanisms possess several advantages such as the possibilities for high acceleration and high accuracy positioning of the end effector. However, most of the proposed parallel manipulators suffer from a limited workspace. In this paper, a novel 6-DOF parallel manipulator with coaxial actuated arms is introduced. Since parallel mechanisms have more workspace limitations compared to that of serial mechanisms, determination of the workspace in parallel manipulators is of the utmost importance. For finding position, angular velocity, and acceleration, in this paper, inverse and forward kinematics of the mechanism are studied and after presenting the workspace limitations, workspace analysis of the hexarot manipulator is performed by using MATLAB software. Next, using the obtained cloud of points from simulation, the overall borders of the workspace are illustrated. Finally, it is shown that this manipulator has the important benefits of combining a large positional workspace in relation to its footprint with a sizable range of platform rotations.

KEYWORDS: Parallel manipulator; Hexarot; Kinematics; Jacobian matrix; Workspace.

1. Introduction

In the design of parallel manipulators, much concern is given to the workspace factor. Parallel mechanisms typically exhibit low inertia, allowing high load capability and high acceleration compared to serial manipulators of the same size. An extensive number of 6-DOF parallel manipulators have been proposed[1–5] after the introduction of Stewart platform manipulator.[6] However, most of the parallel kinematic mechanisms suffer from the small workspace in relation to the manipulator footprint. Moreover, the range of platform rotations is almost always significantly limited compared to serial robots. One approach to increase the size of the positional workspace is to utilize coaxial actuated arms that can rotate infinitely around a central base column.[7] Such mechanisms include the planar manipulators introduced in previous patents[8–10] and research works.[11,13]

Generally, there are many solution methods to solve the robot inverse kinematics problem, for example, analytic solution,[14–18] geometric method,[19] efficient inverse kinematics method,[20] iterative

* Corresponding author. E-mail: s.pedrammehr@gmail.com; spedrammehr@sabanciuniv.edu

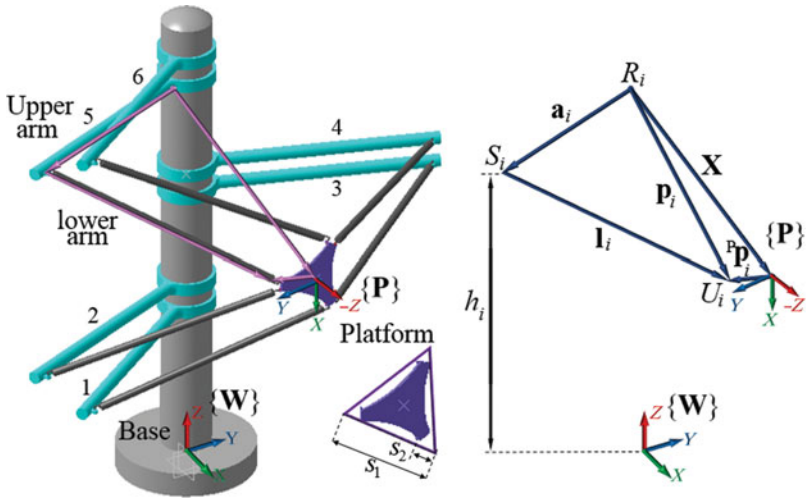

Fig. 1. Hexarot mechanism and the vectorial representation of the *i*th arm.

inverse kinematics method,[21] and screw theory.[22] It is well-known that the forward kinematic solutions of a parallel mechanism is difficult to obtain.[23] This, however, is because the independent equations describing the geometric relationship between different chains which are related to one another in nonlinear manners. Many solutions proposed in the past have concentrated on numerical methods, such as Newton-Raphson,[24,25] and learning networks.[26] By having position inverse solution at hand, a simple way of determining the workspace of a parallel manipulator is to use discretization methods.[27–30] In these methods, the workspace boundary is usually determined in a spherical coordinate system by discretizing the range of azimuth and zenith angles.[31] Bonev and Ryu,[32] Pernkopf and Husty,[33] Huang *et al.*[34], and Gosselin[35] put forward discrete algorithms for calculating position workspace of different six degrees of freedom parallel mechanisms. Majid *et al.*,[36] Tahmasebi and Tsai,[37] Zhu *et al.*[38], and Masory and Wang[39] also studied the workspace of various parallel machine tools by utilizing position inverse solution.

This paper analyses a different 6-DOF platform manipulator based on six coaxial actuated upper arms. Kinematic analysis of a parallel mechanism is the basis for all researches on mechanism, and hence in this research, first inverse and forward kinematic models of hexarot mechanism are developed and also simulated by the code written in MATLAB. The results obtained by theoretical method are further verified by kinematic analysis under Working Model software. Then the limitations of joints and arms are considered in all points of the workspace. Finally, by having the kinematic relations of mechanism and the limitations of workspace at hand, workspace determination is performed by programming and the overall scope of the workspace is displayed in CATIA software.

2. Description of Hexarot Mechanism

The hexarot mechanism consists of a triangular platform, a cylindrical base column, and six actuated rotating arms with coinciding axes of rotation (Fig. 1). Each arm connects by a 5-DOF link to a manipulated platform at its connection point U_i ($i = 1$ to 6). The platform is triangular, and the three pairs of joints on the rotating arms approximately form a triangle. The two triangles compose the two sides of an octahedron. There are six actuated rotational joints R_i between the central cylindrical base column and the upper arms a_i. Each upper arm is connected to a lower arm l_i by a spherical joint S_i. There are six universal joints U_i between the lower arm l_i and the manipulated platform. The location and orientation of the moving platform frame $\{\mathbf{P}\}$ is specified according to the base frame $\{\mathbf{W}\}$. $\mathbf{a}_i$ and $\mathbf{l}_i$ are respectively the length vectors of the upper and lower arms in the base frame of the reference. The physical specifications of the manipulator are presented in the Appendix 1.

The actuators are placed on the base column, and since the lower arms are not susceptible to bending or torsion, so their design can be lightweight. Hence, the total moving mass of the octahedral hexarot is low. The proposed mechanism has six manipulated DOFs. The possibility of using identical drivelines, identical upper arms, and identical lower arm links ensures that the number of different components can be kept low, which would reduce the cost of manufacturing the manipulator. Hexarotcould

https://doi.org/10.1017/S0263574714000988 Published online by Cambridge University Press

be useful in haptics or for working inside cylindrical spaces, such as repairing work inside pipes, positioning, or assembling tasks inside the body of an airplane.

3. Inverse Kinematics

Inverse kinematic problem of the platform involves determination of the rotation, angular velocity, and acceleration of six arms through considering a specified position, velocity, and acceleration of the moving platform center.

Considering a vectorial representation of the mechanism, position vector of the ith spherical joint with the reference in base frame, $\mathbf{a}_i$, can be obtained as:

$$\mathbf{a}_i = \begin{bmatrix} a_i \cos\phi_i & a_i \sin\phi_i & h_i \end{bmatrix}^{\mathrm{T}}, \tag{1}$$

where ϕ_i is the angle between the ith upper arm and X axis of the reference frame $\{\mathbf{W}\}$ and indicates the rotation of ith upper arm around the base column.

Considering the moving platform as an equilateral triangle, and taking into account s_1 as the length of its sides and s_2 as the distance between the universal joint and the vertex, the position of each universal joint, ${}^{P}\mathbf{p}_i$, with reference in frame $\{\mathbf{P}\}$ can be presented as:

$$\begin{aligned}
{}^{\mathrm{P}}\mathbf{p}_1 &= \begin{bmatrix} \frac{(s_1 - s_2)}{2} & \frac{(-s_1 + 3s_2)}{2\sqrt{3}} & 0 \end{bmatrix}^T, \quad {}^{\mathrm{P}}\mathbf{p}_2 = \begin{bmatrix} \frac{s_2}{2} & \frac{(2s_1 - 3s_2)}{2\sqrt{3}} & 0 \end{bmatrix}^T, \\
{}^{\mathrm{P}}\mathbf{p}_3 &= \begin{bmatrix} \frac{(s_1 - 2s_2)}{2} & \frac{-s_1}{2\sqrt{3}} & 0 \end{bmatrix}^T, \quad {}^{\mathrm{P}}\mathbf{p}_4 = \begin{bmatrix} \frac{-(s_1 - 2s_2)}{2} & \frac{-s_1}{2\sqrt{3}} & 0 \end{bmatrix}^T, \\
{}^{\mathrm{P}}\mathbf{p}_5 &= \begin{bmatrix} \frac{-s_2}{2} & \frac{(2s_1 - 3s_2)}{2\sqrt{3}} & 0 \end{bmatrix}^T, \quad {}^{\mathrm{P}}\mathbf{p}_6 = \begin{bmatrix} \frac{-(s_1 - s_2)}{2} & \frac{(-s_1 + 3s_2)}{2\sqrt{3}} & 0 \end{bmatrix}^T.
\end{aligned} \tag{2}$$

These vectors can be expressed in the base frame of reference by a translation and rotation transformation as follows:

$$\mathbf{p}_i = \mathbf{X} + \mathbf{R}\,{}^{\mathrm{P}}\mathbf{p}_i \tag{3}$$

in which $\mathbf{p}_i = [p_{ix}, p_{iy}, p_{iz}]$ is the position of each universal joint in frame $\{\mathbf{W}\}$, $\mathbf{X} = [x, y, z]$ is the position vector of the geometrical center of the moving platform in base frame and $\mathbf{R} = \mathbf{R}_{ZYZ}$ is the rotation matrix which can be obtained as:

$$\mathbf{R} = \begin{bmatrix} \cos\theta_1 \cos\theta_2 \cos\theta_3 - \sin\theta_1 \sin\theta_3 & -\cos\theta_1 \cos\theta_2 \sin\theta_3 - \sin\theta_1 \cos\theta_3 & \cos\theta_1 \sin\theta_2 \\ \sin\theta_1 \cos\theta_2 \cos\theta_3 + \cos\theta_1 \sin\theta_3 & -\sin\theta_1 \cos\theta_2 \sin\theta_3 + \cos\theta_1 \cos\theta_3 & \sin\theta_1 \sin\theta_2 \\ -\sin\theta_2 \cos\theta_3 & \sin\theta_2 \sin\theta_3 & \cos\theta_2 \end{bmatrix} \tag{4}$$

in which θ_1, θ_2 and θ_3 are the Euler angles.

The length of the ith lower arm, l_i, can be expressed as:

$$l_i^2 = |\mathbf{p}_i - \mathbf{a}_i|^2. \tag{5}$$

Substituting Eqs. (1) and (3) into Eq. (5) gives the following equation:

$$d_{i1} + d_{i2} \sin\phi_i + d_{i3} \cos\phi_i = 0 \tag{6}$$

in which

$$\begin{aligned}
d_{i1} = {} & x^2 + y^2 + (z - h_i)^2 - l_i^2 + a_i^2 + p_{ix}^2 + p_{iy}^2 + p_{iz}^2 + 2(z - h_i)\, p_{iz} \cos\theta_2 \\
& - 2(z - h_i)\, p_{ix} \sin\theta_2 \cos\theta_3 + 2z(z - h_i)\, p_{iy} \sin\theta_2 \sin\theta_3 \\
& - 2x\,(p_{ix} \sin\theta_1 \sin\theta_3 + p_{iy} \sin\theta_1 \cos\theta_3 - p_{iz} \cos\theta_1 \sin\theta_2)
\end{aligned}$$

https://doi.org/10.1017/S0263574714000988 Published online by Cambridge University Press

$$+2y\,(p_{ix}\cos\theta_1\sin\theta_3 + p_{iy}\cos\theta_1\cos\theta_3 + p_{iz}\sin\theta_1\sin\theta_2)$$
$$+2x\cos\theta_1\cos\theta_2\cos\theta_3(p_{ix} - p_{iy}) + 2yp_{ix}\sin\theta_1\cos\theta_2\cos\theta_3$$
$$-2yp_{iy}\sin\theta_1\cos\theta_2\sin\theta_3, \tag{7}$$

$$d_{i2} = -2a_i(y + p_{ix}\cos\theta_1\sin\theta_3 + p_{iy}\cos\theta_1\cos\theta_3 + p_{iz}\sin\theta_1\sin\theta_2$$
$$+ p_{ix}\sin\theta_1\cos\theta_2\cos\theta_3 - p_{iy}\sin\theta_1\cos\theta_2\sin\theta_3), \tag{8}$$

$$d_{i3} = -2a_i(x - p_{ix}\sin\theta_1\sin\theta_3 - p_{iy}\sin\theta_1\cos\theta_3 + p_{iz}\cos\theta_1\sin\theta_2$$
$$+ p_{ix}\cos\theta_1\cos\theta_2\cos\theta_3 - p_{iy}\cos\theta_1\cos\theta_2\sin\theta_3). \tag{9}$$

ϕ_i can be obtained by substituting Eqs. (7)–(9) into Eq. (6), which yields:

$$\phi_i = -2\arctan\left[\left(d_{i2} - \sqrt{-d_{i1}^2 + d_{i2}^2 + d_{i3}^2}\right)\Big/ d_{i1} - d_{i3}\right] \quad \text{for } i = 1, 2, 5, 6,$$
$$\phi_i = -2\arctan\left[\left(d_{i2} + \sqrt{-d_{i1}^2 + d_{i2}^2 + d_{i3}^2}\right)\Big/ d_{i1} - d_{i3}\right] \quad \text{for } i = 3,\ 4. \tag{10}$$

Considering Eq. (3), $\mathbf{a}_i$ can be obtained as:

$$\mathbf{l}_i = \mathbf{X} + \mathbf{R}^{\mathrm{P}}\mathbf{p}_i - \mathbf{a}_i. \tag{11}$$

Considering $\mathbf{n}_i$ as the unit vector of the ith lower arm (i.e., $\mathbf{l}_i = l_i\mathbf{n}_i$) and taking the derivative with respect to time on both sides of Eq. (11), and then taking the derivative with respect to time on both sides of the resulting equation, yields:

$$(\mathbf{a}_i \times \mathbf{n}_i)\,.\,\dot{\boldsymbol{\varphi}}_i = \dot{\mathbf{X}} \cdot \mathbf{n}_i + (\mathbf{R}^{\mathrm{P}}\mathbf{p}_i \times \mathbf{n}_i) \cdot \omega, \tag{12}$$

where $\dot{\mathbf{X}}$ and $\boldsymbol{\omega}$ are, respectively, the linear and angular velocity of the moving platform center in the base frame. $\dot{\boldsymbol{\varphi}}_i$ is also the angular velocity of the ith upper arm.

The angular velocity of upper arm is only in the Z direction. Therefore, only the Z parameter of $(\mathbf{a}_i \times \mathbf{n}_i)$ will be considered in the dot product of $\dot{\boldsymbol{\varphi}}_i$. By considering an_{zi} as the Z parameter of $(\mathbf{a}_i \times \mathbf{n}_i)$, this parameter can be defined as:

$$an_{zi} = a_i n_{iy}\cos\phi_i - a_i n_{ix}\sin\phi_i. \tag{13}$$

The angular velocity of the ith upper arm can be obtained by substituting Eq. (13) into Eq. (12), which yields:

$$\dot{\boldsymbol{\varphi}} = \mathbf{J}^{-1}\begin{bmatrix}\dot{\mathbf{X}} \\ \omega\end{bmatrix} \tag{14}$$

in which $\mathbf{J}^{-1}$ is the inverse Jacobian matrix and can be expressed as:

$$\mathbf{J}^{-1} = \begin{bmatrix}(\mathbf{n}_1/an_{z1})^{\mathrm{T}} & (\mathbf{R}^{\mathrm{P}}\mathbf{p}_1 \times \mathbf{n}_1/an_{z1})^{\mathrm{T}} \\ \vdots & \vdots \\ (\mathbf{n}_6/an_{z6})^{\mathrm{T}} & (\mathbf{R}^{\mathrm{P}}\mathbf{p}_6 \times \mathbf{n}_6/an_{z6})^{\mathrm{T}}\end{bmatrix}_{6\times 6}. \tag{15}$$

Taking the derivative of Eq. (14) with respect to time, the angular acceleration of the ith upper arm, $\ddot{\phi}_i$, can be calculated from:

$$\ddot{\phi}_i(a_i n_{iy}\cos\phi_i - a_i n_{ix}\sin\phi_i) - \dot{\phi}_i(a_i n_{ix}\dot{\phi}_i\cos\phi_i + a_i n_{iy}\dot{\phi}_i\sin\phi_i)$$
$$+\dot{\phi}_i(a_i n_{ix}\omega_{lzi}\cos\phi_i + a_i n_{iy}\omega_{lzi}\sin\phi_i - a_i n_{iz}\omega_{lyi}\sin\phi_i - a_i n_{iz}\omega_{lxi}\cos\phi_i)$$
$$= \{\ddot{\mathbf{X}} + (\boldsymbol{\omega}\times\dot{\mathbf{X}}) + (\dot{\mathbf{X}}\times\boldsymbol{\omega}_{li}) + [\boldsymbol{\omega}\times(\boldsymbol{\omega}\times\mathbf{R}^{\mathrm{P}}\mathbf{p}_i) + (\boldsymbol{\omega}\times\mathbf{R}^{\mathrm{P}}\mathbf{p}_i)\times\boldsymbol{\omega}_{li}] + (\boldsymbol{\alpha}\times\mathbf{R}^{\mathrm{P}}\mathbf{p}_i)\}\cdot\mathbf{n}_i \tag{16}$$

https://doi.org/10.1017/S0263574714000988 Published online by Cambridge University Press

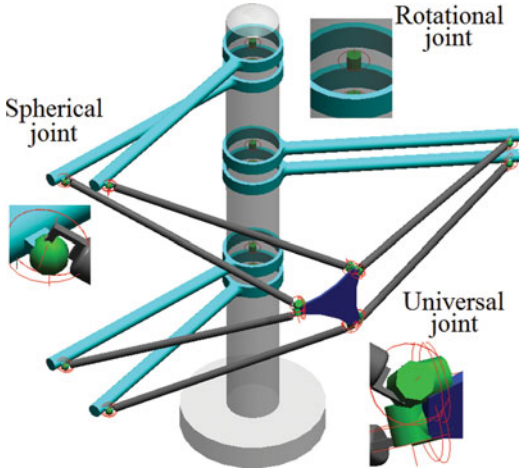

Fig. 2. Hexarot model in Working Model software, and relevant joint elements and chords.

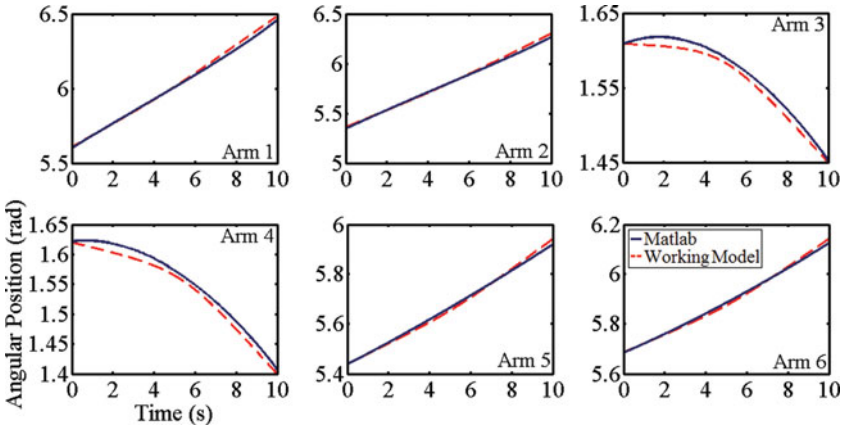

Fig. 3. Path 1; angular positions of six upper arms obtained by analytical approach and Working Model software.

where $\ddot{\mathbf{X}}$ and $\boldsymbol{\alpha}$ are, respectively, the linear and angular acceleration of the moving platform center in the base frame of reference and $\boldsymbol{\omega}_{li} = [\,\omega_{lxi}\ \omega_{lyi}\ \omega_{lzi}\,]^{\mathrm{T}}$ is the angular velocity of the ith lower arm.

In order to demonstrate the results of the formulation, a case study is performed for a typical hexarot mechanism with physical specifications presented in Appendix 1. For this purpose, the formulation has been implemented in a programme written in MATLAB for inverse kinematics of hexarot parallel manipulator. Initial conditions taken for the simulations are given in Appendix 2.

At first, a simple straight line path with a constant velocity profile is considered and the orientation of the platform is conserved during the simulation (Path 1, Appendix 2). The angular positions, velocities and accelerations of the six arms obtained by the current model are simulated. In order to corroborate the results of analytical method, kinematics of the six arms are also obtained by using Working Model software (Design Simulation Technologies, Inc.). For this purpose, a three-dimensional model of the mechanism was developed in Solidworks. The model was exported to Working Model software and collisions between bodies were deactivated. Joint elements were created and relevant boundary conditions were applied (Fig. 2). Finally, kinematic analysis was performed to obtain positions, velocities and accelerations of the six arms. The results of both simulations are illustrated in Figs. 3–5, respectively.

Figure 3 illustrates the displacement of the six arms during simple time dependent motion of the platform from its reference point to the final position in 10 s. It is shown that the arms 1, 2, 5, and 6 move counter clock wise, while the arms 3 and 4 move in the opposite direction to satisfy the mentioned path. Moreover, Figs. 4 and 5, respectively, show the change in angular velocity and acceleration of the six arms during motion in the mentioned path. The results of simulation under

https://doi.org/10.1017/S0263574714000988 Published online by Cambridge University Press

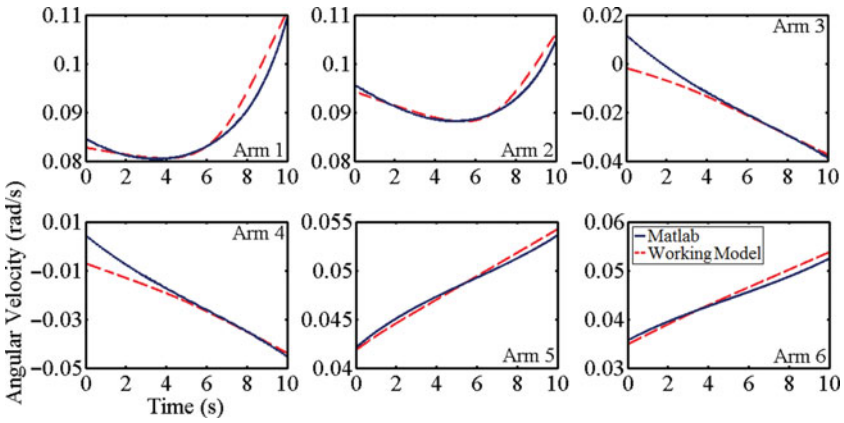

Fig. 4. Path 1; angular velocities of six upper arms obtained by analytical approach and Working Model software.

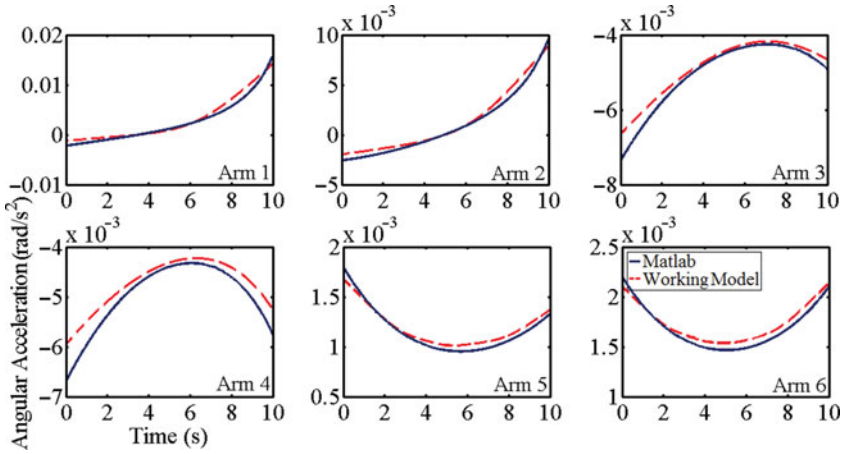

Fig. 5. Path 1; angular accelerations of six upper arms obtained by analytical approach and Working Model software.

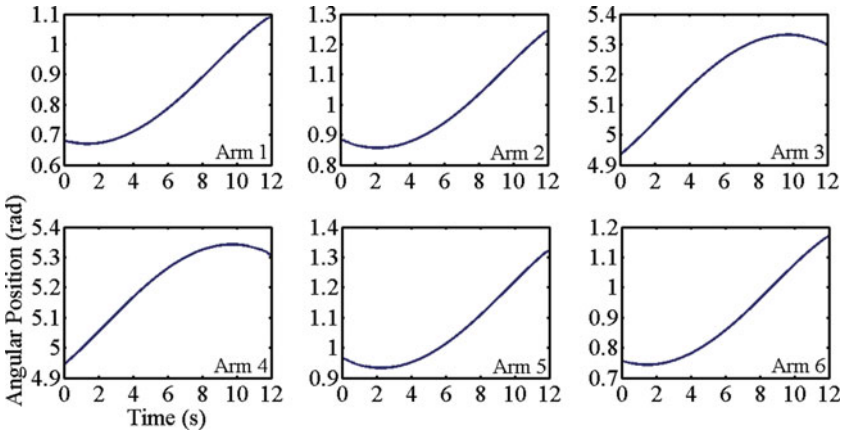

Fig. 6. Path 2; angular positions of six upper arms obtained by analytical approach.

MATLAB have also been verified by the simulation of the same path under Working Model software, and the results of both simulation methods are in good agreement.

In order to further investigate the kinematic characteristics of six arms, a circular path with constant speed is used for computer simulation. Moreover, the orientation of the moving platform is

https://doi.org/10.1017/S0263574714000988 Published online by Cambridge University Press

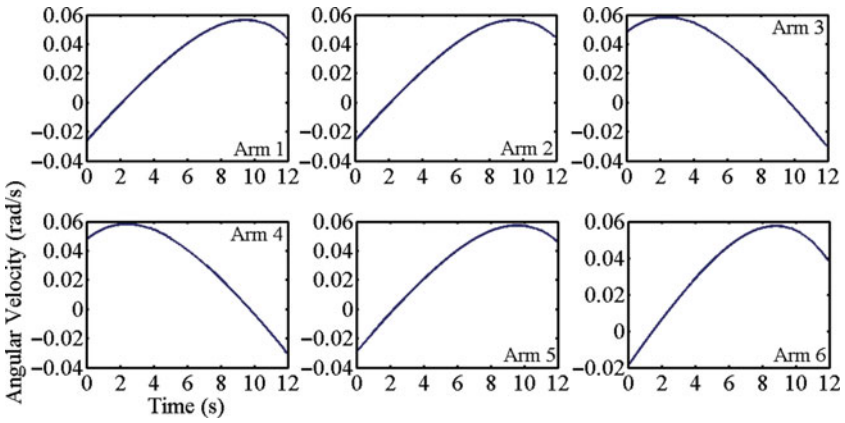

Fig. 7. Path 2; angular velocities of six upper arms obtained by analytical approach.

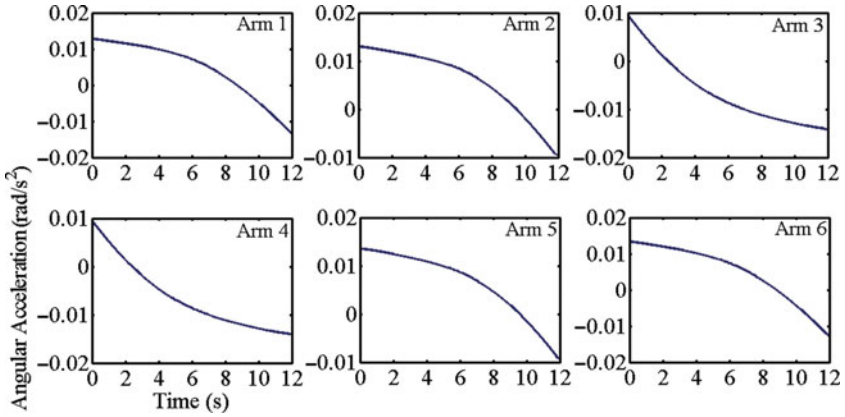

Fig. 8. Path 2; angular accelerations of six upper arms obtained by analytical approach.

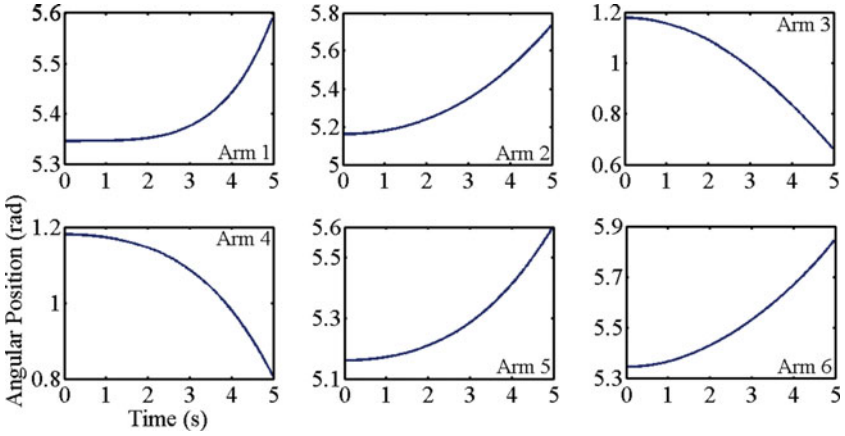

Fig. 9. Path 3; angular positions of six upper arms obtained by analytical approach.

kept unchanged during the simulation (Path 2, Appendix 2). The results of simulation for motion of platform in circular path are illustrated in Figs. 6–8.

In Path 3 (Appendix 2), to consider a realistic motion of hexarot mechanism, a screwing motion of platform with constant acceleration is taken into account. This motion, moreover, requires rolling and displacement of the platform including changes in position and orientation of the platform simultaneously. The results for the motion of the platform in the third path are presented in Figs. 9–11 for angular position, velocity, and acceleration of the platform, respectively.

https://doi.org/10.1017/S0263574714000988 Published online by Cambridge University Press

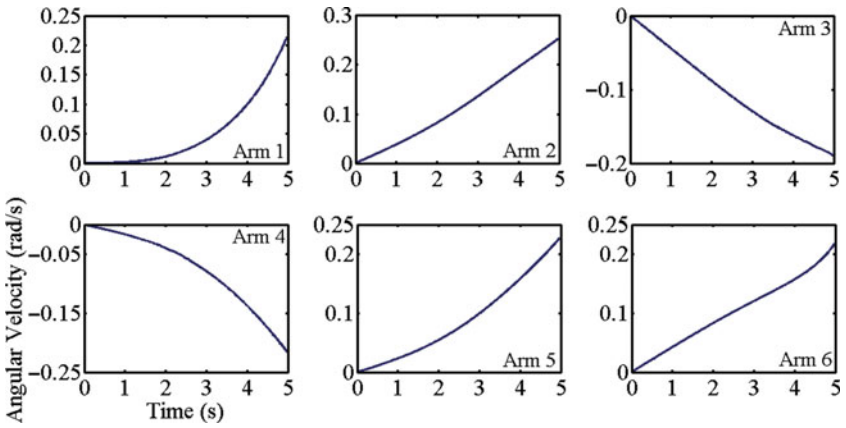

Fig. 10. Path 3; angular velocities of six upper arms obtained by analytical approach.

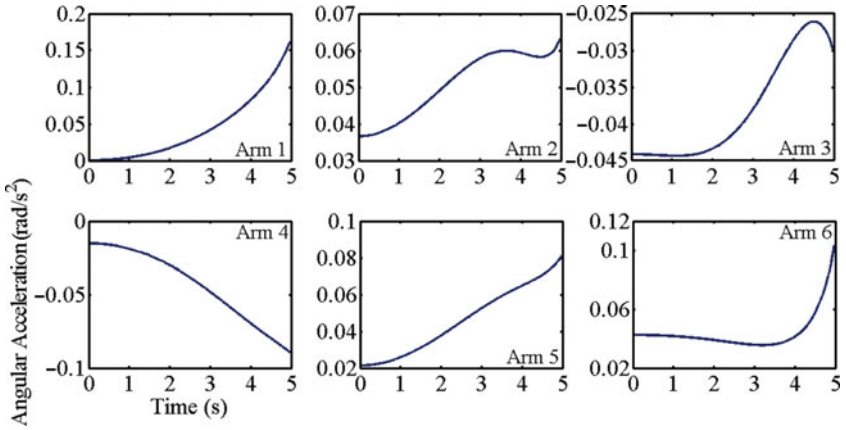

Fig. 11. Path 3; angular accelerations of six upper arms obtained by analytical approach.

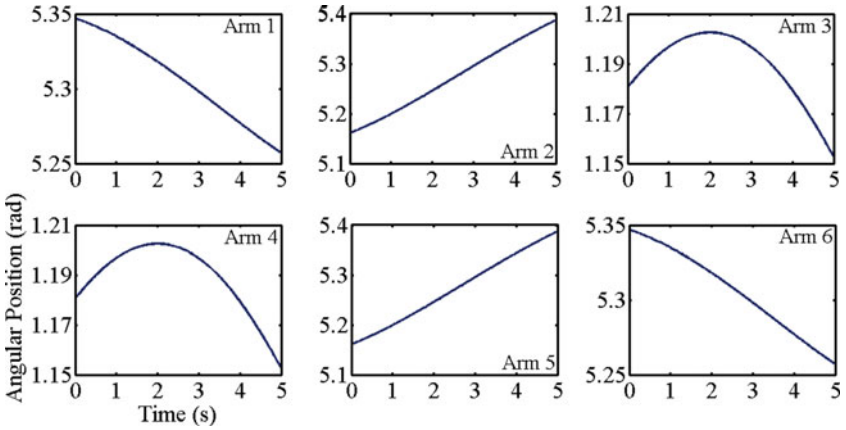

Fig. 12. Path 4; angular positions of six upper arms obtained by analytical approach.

In order to check the kinematic characteristics of six arms under change in orientation of platform and without any change in its position, yawing is considered for platform motion (Path 4, Appendix 2). It should be noted that this motion is one of the most preferred motions of 6-DOF mechanisms, in which the position remains constant and the orientation changes with constant angular velocity. Figures 12–14 respectively illustrates changes in angular position, velocity, and acceleration of the arms during yawing motion.

https://doi.org/10.1017/S0263574714000988 Published online by Cambridge University Press

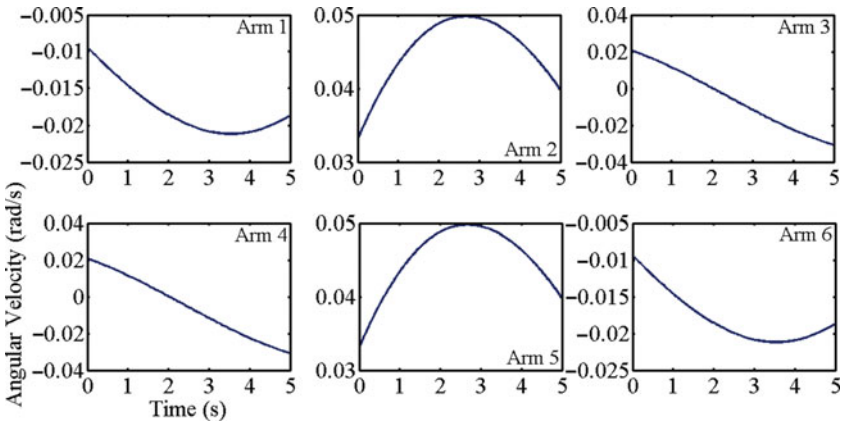

Fig. 13. Path 4; angular velocities of six upper arms obtained by analytical approach.

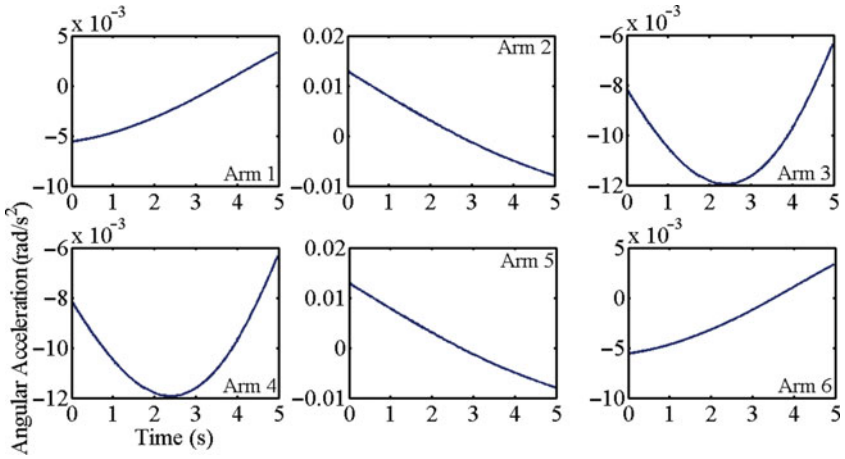

Fig. 14. Path 4; angular accelerations of six upper arms obtained by analytical approach.

4. Forward Kinematics

The forward kinematic problem of the platform is to determine of the position, velocity, and acceleration of the moving platform center through considering a specified rotation, angular velocity, and acceleration of the six arms. Therefore, in forward kinematics unknown parameters are divided in to two groups of position and orientation of the moving platform. Therefore, there will be six unknown parameters which are x, y, z, θ_1, θ_2, and θ_3.

By substituting Eqs. (7)–(9) into Eq. (6), the function $f_i(x_n)$ can be expressed as:

$$\begin{aligned} f_i(x_n) = \varepsilon_i = {} & x^2 + y^2 + (z - h_i)^2 - l_i^2 + a_i^2 + p_{ix}^2 + p_{iy}^2 + p_{iz}^2 + 2(z - h_i)\, p_{iz} \cos\theta_2 \\ & - 2(z - h_i)\, p_{ix} \sin\theta_2 \cos\theta_3 + 2z(z - h_i)\, p_{iy} \sin\theta_2 \sin\theta_3 \\ & - 2x\,(p_{ix} \sin\theta_1 \sin\theta_3 + p_{iy} \sin\theta_1 \cos\theta_3 - p_{iz} \cos\theta_1 \sin\theta_2) \\ & + 2y\,(p_{ix} \cos\theta_1 \sin\theta_3 + p_{iy} \cos\theta_1 \cos\theta_3 + p_{iz} \sin\theta_1 \sin\theta_2) \\ & + 2x \cos\theta_1 \cos\theta_2 \cos\theta_3 (p_{ix} - p_{iy}) + 2y p_{ix} \sin\theta_1 \cos\theta_2 \cos\theta_3 \\ & - 2y p_{iy} \sin\theta_1 \cos\theta_2 \sin\theta_3 - 2a_i \sin\phi_i (y + p_{ix} \cos\theta_1 \sin\theta_3 + p_{iy} \cos\theta_1 \cos\theta_3 \\ & + p_{iz} \sin\theta_1 \sin\theta_2 + p_{ix} \sin\theta_1 \cos\theta_2 \cos\theta_3 - p_{iy} \sin\theta_1 \cos\theta_2 \sin\theta_3) \\ & - 2a_i \cos\phi_i (x - p_{ix} \sin\theta_1 \sin\theta_3 - p_{iy} \sin\theta_1 \cos\theta_3 + p_{iz} \cos\theta_1 \sin\theta_2 \\ & + p_{ix} \cos\theta_1 \cos\theta_2 \cos\theta_3 - p_{iy} \cos\theta_1 \cos\theta_2 \sin\theta_3) \end{aligned} \tag{17}$$

https://doi.org/10.1017/S0263574714000988 Published online by Cambridge University Press

in which ε_i is the error for coordination of the ith joint. The output of forward kinematics is $\mathbf{X} = [\,x\ y\ z\ \theta_1\ \theta_2\ \theta_3\,]^{\mathrm{T}}$. By replacing the value of $\mathbf{X}$ in Eq. (17), the evaluation function is determined and the more $\mathbf{X}$ approaches to its real value, the more the function approaches to zero, so that error stays in the desired domain. Regarding six rotating joints, it should be noted that Eq. (17) must be used for calculation of each joint.

In this study, for solving the equation, the Newton-Raphson method is utilized, because this method only needs repeating the prior calculation. This feature leads to stability of the calculations and also to convergence of the method hence producing the final answer in less time and with less errors.

$$f_i(x) = f_i'(x)\,[x_{n+1} - x_n]\,, \tag{18}$$

where x_n and x_{n+1} are respectively the available values and the value obtained from x_n. $f_i'(x)$ is the fractional derivative of $f_i(x_n)$ which can be calculated as:

$$f_i'(x_n) = \frac{\partial f_i(x_n)}{\partial x_n} = \frac{\partial \varepsilon_i}{\partial x_n} = \begin{bmatrix} \frac{\partial \varepsilon_1}{\partial x_n} & \frac{\partial \varepsilon_1}{\partial y_n} & \frac{\partial \varepsilon_1}{\partial z_n} & \frac{\partial \varepsilon_1}{\partial \theta_{1n}} & \frac{\partial \varepsilon_1}{\partial \theta_{2n}} & \frac{\partial \varepsilon_1}{\partial \theta_{3n}} \\ \vdots & \vdots & \vdots & \vdots & \vdots & \vdots \\ \frac{\partial \varepsilon_6}{\partial x_n} & \frac{\partial \varepsilon_6}{\partial y_n} & \frac{\partial \varepsilon_6}{\partial z_n} & \frac{\partial \varepsilon_6}{\partial \theta_{1n}} & \frac{\partial \varepsilon_6}{\partial \theta_{2n}} & \frac{\partial \varepsilon_6}{\partial \theta_{3n}} \end{bmatrix}_{6\times 6}, \tag{19}$$

which yields:

$$\begin{aligned} \frac{\partial \varepsilon_i}{\partial x} &= 2x - 2p_{ix}\sin\theta_1\sin\theta_3 - 2p_{iy}\sin\theta_1\cos\theta_3 + 2p_{iz}\cos\theta_1\sin\theta_2 \\ &\quad + 2p_{ix}\cos\theta_1\cos\theta_2\cos\theta_3 - 2p_{iy}\cos\theta_1\cos\theta_2\sin\theta_3 - 2a_i\cos\phi_i\,, \end{aligned} \tag{20}$$

$$\begin{aligned} \frac{\partial \varepsilon_i}{\partial y} &= 2y - 2p_{ix}\cos\theta_1\sin\theta_3 - 2p_{iy}\cos\theta_1\cos\theta_3 + 2p_{iz}\sin\theta_1\sin\theta_2 \\ &\quad + 2p_{ix}\sin\theta_1\cos\theta_2\cos\theta_3 - 2p_{iy}\sin\theta_1\cos\theta_2\sin\theta_3 - 2a_i\sin\phi_i\,, \end{aligned} \tag{21}$$

$$\frac{\partial \varepsilon_i}{\partial z} = 2z - 2h_i + 2p_{iz}\cos\theta_2 + 2p_{iy}\sin\theta_2\sin\theta_3 - 2p_{iz}\cos\theta_1\sin\theta_2 - 2p_{ix}\cos\theta_1\cos\theta_2\cos\theta_3, \tag{22}$$

$$\begin{aligned} \frac{\partial \varepsilon_i}{\partial \theta_1} &= 2x\,(p_{ix}\cos\theta_1\sin\theta_3 - p_{iy}\cos\theta_1\cos\theta_3 - p_{iz}\sin\theta_1\sin\theta_3) \\ &\quad - 2y(p_{ix}\sin\theta_1\sin\theta_3 + p_{iy}\sin\theta_1\cos\theta_3 - p_{iz}\cos\theta_1\sin\theta_2) \\ &\quad + 2y\cos\theta_1\cos\theta_2\cos\theta_3(p_{ix} - p_{iy}) - 2xp_{ix}\sin\theta_1\cos\theta_2\cos\theta_3 \\ &\quad + 2xp_{iy}\sin\theta_1\cos\theta_2\sin\theta_3 + 2a_i\sin\phi_i(p_{ix}\sin\theta_1\sin\theta_3 + p_{iy}\sin\theta_1\cos\theta_3 \\ &\quad - p_{iz}\cos\theta_1\sin\theta_2 - p_{ix}\cos\theta_1\cos\theta_2\cos\theta_3 + p_{iy}\cos\theta_1\cos\theta_2\sin\theta_3) \\ &\quad + 2a_i\cos\phi_i(p_{ix}\cos\theta_1\sin\theta_3 + p_{iy}\cos\theta_1\cos\theta_3 + p_{iz}\sin\theta_1\sin\theta_2 \\ &\quad + p_{ix}\sin\theta_1\cos\theta_2\cos\theta_3 - p_{iy}\sin\theta_1\cos\theta_2\cos\theta_3), \end{aligned} \tag{23}$$

$$\begin{aligned} \frac{\partial \varepsilon_i}{\partial \theta_2} &= 2p_{iz}(h_i - z)\,\sin\theta_2 + 2xp_{iz}\cos\theta_1\cos\theta_2 + 2yp_{iz}\sin\theta_1\cos\theta_2 + 2zp_{ix}\cos\theta_2\cos\theta_3 \\ &\quad + 2zp_{iy}\cos\theta_1\sin\theta_3 + 2h_ip_{ix}\cos\theta_2\cos\theta_3 - 2h_ip_{iy}\cos\theta_2\sin\theta_3 - 2xp_{ix}\cos\theta_1\sin\theta_2\cos\theta_3 \\ &\quad + 2xp_{iy}\cos\theta_1\sin\theta_2\sin\theta_3 - 2yp_{ix}\sin\theta_1\sin\theta_2\cos\theta_3 + 2yp_{iy}\sin\theta_1\sin\theta_2\sin\theta_3 \\ &\quad - 2a_i\sin\phi_i(-p_{ix}\sin\theta_1\sin\theta_2\cos\theta_3 + p_{iy}\sin\theta_1\sin\theta_2\sin\theta_3 + p_{iz}\sin\theta_1\cos\theta_2) \\ &\quad - 2a_i\cos\phi_i(-p_{ix}\cos\theta_1\sin\theta_2\cos\theta_3 + p_{iy}\cos\theta_1\sin\theta_2\sin\theta_3 + p_{iz}\cos\theta_1\cos\theta_2), \end{aligned} \tag{24}$$

https://doi.org/10.1017/S0263574714000988 Published online by Cambridge University Press

$$\frac{\partial \varepsilon_i}{\partial \theta_3} = -2xp_{ix}\cos\theta_1\cos\theta_3 + 2xp_{iy}\sin\theta_1\sin\theta_3 + 2yp_{ix}\cos\theta_1\cos\theta_3$$
$$- 2yp_{iy}\cos\theta_1\sin\theta_3 - 2zp_{ix}\sin\theta_2\sin\theta_3 + 2zp_{iy}\sin\theta_2\sin\theta_3$$
$$- 2h_i p_{ix}\sin\theta_2\sin\theta_3 - 2h_i p_{iy}\sin\theta_2\cos\theta_3 - 2xp_{ix}\cos\theta_1\cos\theta_2\sin\theta_3$$
$$- 2xp_{iy}\cos\theta_1\cos\theta_2\cos\theta_3 - 2yp_{ix}\sin\theta_1\cos\theta_2\sin\theta_3 - 2yp_{iy}\sin\theta_1\cos\theta_2\cos\theta_3$$
$$- 2a_i\sin\phi_i(p_{ix}\cos\theta_1\cos\theta_3 - p_{ix}\sin\theta_1\cos\theta_2\sin\theta_3 - p_{iy}\cos\theta_1\sin\theta_3$$
$$- p_{iy}\sin\theta_1\cos\theta_2\sin\theta_3) - 2a_i\cos\phi_i(p_{ix}\sin\theta_1\cos\theta_3 - p_{ix}\cos\theta_1\cos\theta_2\sin\theta_3$$
$$+ p_{iy}\sin\theta_1\sin\theta_3 - p_{iy}\cos\theta_1\cos\theta_2\cos\theta_3). \tag{25}$$

By substituting Eqs. (20) to (25) into Eq. (19) and then by substituting the resulting equation and Eq. (17) into Eq. (18), x_{n+1} can be calculated from x_n.

In this step, there are six linear equations and six unknown parameters in which using the Gauss-Jordan method, it is possible to obtain x_{n+1} from x_n. This repeating continues till the error get in the desired domain which is assumed to be 10^{-3} (mm) in this study.

Taking the product of the two sides of Eq. (14) with an_{zi} **J**, gives:

$$\begin{bmatrix} \dot{\mathbf{X}} \\ \boldsymbol{\omega} \end{bmatrix} = an_{zi}\mathbf{J}\dot{\boldsymbol{\phi}}. \tag{26}$$

Therefore, using the Jacobin matrix, which is obtained from the position of the platform, and using the angular velocity of the spherical joints as well, it is possible to calculate the velocity of the moving platform center.

Considering:

$$u_i = a_i n_{iy}\omega_{lzi}\sin\phi_i - a_i n_{iz}\omega_{lyi}\sin\phi_i + a_i n_{ix}\omega_{lzi}\cos\phi_i$$
$$- a_i n_{iz}\omega_{lxi}\cos\phi_i - a_i n_{ix}\dot{\phi}_i\cos\phi_i - a_i n_{iy}\dot{\phi}_i\sin\phi_i \tag{27}$$

and taking the product of the two sides of Eq. (16) with **J**, gives:

$$\begin{bmatrix} \ddot{\mathbf{X}} \\ \boldsymbol{\alpha} \end{bmatrix} = \mathbf{J}(an_{zi}\ddot{\phi}_i) + \mathbf{J}(u_i\dot{\phi}_i) - \mathbf{J}\frac{\mathrm{d}\mathbf{J}^{-1}}{\mathrm{d}t}\begin{bmatrix} \dot{\mathbf{X}} \\ \boldsymbol{\omega} \end{bmatrix} \tag{28}$$

Therefore, using the Jacobin matrix, which is obtained from moving platform position, and using the angular velocity and acceleration of spherical joints as well as velocity of the platform, it is possible to calculate the acceleration of moving platform center.

5. Workspace Limitations

In parallel mechanism, finding the workspace has limitations in which all of the conditions must take into consideration for all points. These limitations lie in to two parts including joints and arms. In this section, the limitations due to the joints are considered and in the next step, the limitations of the arms will be discussed.

5.1. Limitations existed in joints

In this mechanism, there are three kinds of joints, thus there will be three limitations. The first kind is rotational joint in which mechanism force is fulfilled by this joint. Angle of these joints about X axis of the mechanism coordinate system is determined using Eqs. (7)–(10). For joints including 1, 2, 5, and 6 it must be $0 < \phi_i < \pi/2$ and for joints 3 and 4 it must be $-\pi/2 < \phi_i < 0$. If the ϕ_i for rotational arms exceeds the values, then lack of alignment in arms attached to each other in vectorial chain will lead to aligning of forces applied to the arms fixed to the platform and consequently bending and buckling effects in the joints will be increased.

https://doi.org/10.1017/S0263574714000988 Published online by Cambridge University Press

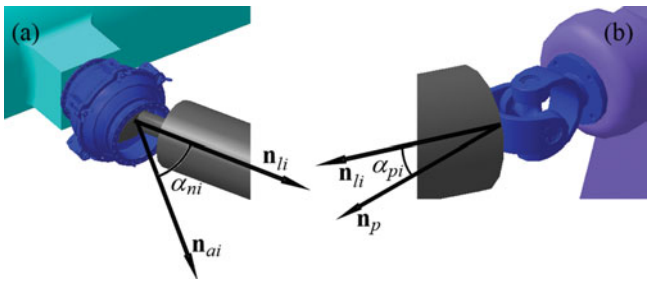

Fig. 15. (a) Spherical joint between upper and lower arms; (b) universal joint between lower arms and manipulated platform.

The second type of joints used in the mechanism is spherical joint which provides three degrees of freedom movement (Fig. 15a).

In Fig. 15, $\mathbf{n}_{li}$ is the unit vector of ith lower arm (i.e., $\mathbf{n}_{li} = \mathbf{l}_i/l_i$). $\mathbf{n}_{ai}$ is also the unit vector normal to the ith upper arm and can be expressed as follows:

$$\begin{aligned} \mathbf{n}_{ai} &= [\sin\phi_i \quad -\cos\phi_i \quad 0]^{\mathrm{T}} \quad \text{for } i = 1, 2, 5, 6, \\ \mathbf{n}_{ai} &= [-\sin\phi_i \quad \cos\phi_i \quad 0]^{\mathrm{T}} \quad \text{for } i = 3,\ 4. \end{aligned} \tag{29}$$

α_{ni} is the angle between $\mathbf{n}_{ai}$ and $\mathbf{n}_{li}$, and can be obtained as:

$$\alpha_{ni} = \cos^{-1}(\mathbf{n}_{ai} \cdot \mathbf{n}_{li}). \tag{30}$$

Regarding the rotational limitation of the spherical joints, the value of this angle is between 0 and $\pi/2$.

The third type of joints used in the mechanism is universal joints with two degree of freedom which fix lower arms to platform (Fig. 15b).

$\mathbf{n}_p$ is the unit vector which is normal to the platform, and can be obtained as:

$$\mathbf{n}_p = ({}^{\mathrm{P}}p_4 - {}^{\mathrm{P}}p_1) \times ({}^{\mathrm{P}}p_5 - {}^{\mathrm{P}}p_1). \tag{31}$$

α_{pi} is also the angle between the inverse direction of $\mathbf{n}_{li}$ and $\mathbf{n}_p$, and can be obtained as:

$$\alpha_{pi} = \cos^{-1}\left[(-\mathbf{n}_{li}) \cdot \mathbf{n}_p\right]. \tag{32}$$

5.2. Limitations existed in arms

There are two kinds of limitations in arms of this mechanism. The first limitation is due to the length of arms, in which, in a specified configuration, the lengths of arms obtained from inverse kinematic equations, must not exceed the value obtained by designer. For this purpose, the arm length, l_i, is calculated by Eq. (5) and compared with its real value. If the theoretical value for arm length is more than the real length of arm, then the considered point lies out of workspace.

The second limitation is due to the collision of the arms which is classified into three groups. The first is lower arms to upper arms collision. In this case there is a possibility of collision between arms including: a_1 with l_2, a_2 with l_1, a_3 with l_4, a_4 with l_3, a_5 with l_6, a_6 with l_5, a_2 with l_5, and a_5 with l_2. The second one is due to potential collision of lower arms to each other. In this case there is a possibility of collision between arms including: l_1 with l_2, l_3 with l_4, l_5 with l_6, and l_2 with l_5. The third one is the possible collision between lower arms and the base. Therefore, each type of the collisions have to be taken into account to obtain the existence of a point in workspace.

Considering all the base column and the upper and lower arms as cylindrical bodies, and vectors $\mathbf{u}_B$ and $\mathbf{v}_B$ as the point to the endpoints of the centerline of each body. All positions on the centerline

https://doi.org/10.1017/S0263574714000988 Published online by Cambridge University Press

of each body, $\mathbf{c}_B$, can be described as:

$$\mathbf{c}_B = \mathbf{u}_B + S_B(\mathbf{v}_B - \mathbf{u}_B). \tag{33}$$

Equation (33) is obtained in order to consider the collision of the arms in which $0 \leq S_B \leq 1$.

The position vector between the centerline of two bodies B_i and B_j is called $\mathbf{B}_{ij}$ and can be obtained as:

$$\mathbf{B}_{ij} = \mathbf{c}_{Bj} - \mathbf{c}_{Bi} = \mathbf{u}_{Bj} - \mathbf{u}_{Bi} + S_{Bj}(\mathbf{v}_{Bj} - \mathbf{u}_{Bj}) - S_{Bi}(\mathbf{v}_{Bi} - \mathbf{u}_{Bi}). \tag{34}$$

In Equation (34), variables including S_{Bi} and S_{Bj} are unknown. Using the concept of finding extremes of two variable functions, the minimum answer of Eq. (34) can be obtained by taking the derivative with respect to the both S_{Bi} and S_{Bj} from the two sides of the equation, and equaling the resulting equation with zero which gives a system of two equations, as:

$$\begin{cases} \left[(v_{Bjx} - u_{Bjx})(u_{Bix} - v_{Bix}) + (v_{Bjy} - u_{Bjy})(u_{Biy} - v_{Biy}) + (v_{Bjz} - u_{Bjz})(u_{Biz} - v_{Biz})\right] S_{Bj} \\ \quad + \left[(u_{Bix} - v_{Bix})^2 + (u_{Biy} - v_{Biy})^2 + (u_{Biz} - v_{Biz})^2\right] S_{Bi} \\ = (v_{Bix} - v_{Bjx})(v_{Bix} - u_{Bix}) + (v_{Biy} - v_{Bjy})(v_{Biy} - u_{Biy}) + (v_{Biz} - v_{Bjz})(v_{Biz} - u_{Biz}) \\ \left[(u_{Bix} - v_{Bix})(v_{Bjx} - u_{Bjx}) + (u_{Biy} - v_{Biy})(v_{Bjy} - u_{Bjy}) + (u_{Biz} - v_{Biz})(v_{Bjz} - u_{Bjz})\right] S_{Bi} \\ \quad + \left[(v_{Bjx} - u_{Bjx})^2 + (v_{Bjy} - u_{Bjy})^2 + (v_{Bjz} - u_{Bjz})^2\right] S_{Bj} \\ = (v_{Bix} - v_{Bjx})(u_{Bix} - v_{Bix}) + (v_{Biy} - v_{Bjy})(u_{Biy} - v_{Biy}) + (v_{Biz} - v_{Bjz})(u_{Biz} - v_{Biz}). \end{cases} \tag{35}$$

The minimum distance of the two bodies B_i and B_j can be obtained by substituting S_{Bi} and S_{Bj} which are obtained from Eq. (35) into Eq. (34).

By considering $\mathbf{r}_{Bi}$ and $\mathbf{r}_{Bj}$ as two radiuses of the body, if $\left|\mathbf{B}_{ij}\right|_{\min} > \mathbf{r}_{Bi} + \mathbf{r}_{Bj}$ then there will be no collision and considered point exists in the workspace. It should be noted that the considered condition should be checked for all 18 cases so that lack of collision would be verified.

5.3. Singular conditions

If the determinant of the inverse Jacobian matrix in Eq. (15) equals to zero, $\det(\mathbf{J}^{-1}) = 0$, the platform will be in singular point which cannot be considered as a point within the workspace. In the mentioned condition, manipulator gains extra DOFs and goes to be out of control. Moreover, when the determinant of the forward kinematics Jacobian matrix in Eq. (26) equals to zero, $\det(\mathbf{J}) = 0$, other possible singular conditions occur which reduce the DOFs of the mechanism. Note that in some configurations both the determinants of the inverse and forward kinematics Jacobian matrices may be zero. This, therefore, is synthetic singular condition which can be expressed as having platform motion in situation when there are no actuating forces, or when there are the actuation forces in the arms without any motion of the platform.

In order to investigate the singularity-free workspace of the mechanism, when the above mentioned determinants become less than 0.001, i.e., $\det(\mathbf{J}^{-1}) < 0.001$ or $\det(\mathbf{J}) < 0.001$, the point is considered as a singular point and not taken into account as a point within the workspace of the mechanism.

6. Manipulator Workspace

In order to assign a whole gamut of workspace, 10 different configurations are chosen and illustrated in Fig. 16 (all the quantities are given in SI units). This figure includes (a) reference configuration, closed arms (0.6, 0, 1.275) without change in orientation (0, 0, 0); (b) upmost position, maximum in Z direction (0.8, 0, 1.8), orientation kept unchanged (0, 0, 0); (c) maximum in Y direction and the nearest to the reference (0.8, −0.3, 1.275), without change in orientation (0, 0, 0); (d) maximum possible rotation in all directions ($\pi/4$,$\pi/4$,$\pi/4$), without change in YZ plane and the nearest to the reference (0.8, 0, 1.275); (e) maximum possible rotation in all directions ($\pi/4$,$\pi/4$,$\pi/4$) without change in YZ plane and the farthest to the reference (1.6, 0, 1.275); (f) maximum possible rotation in all directions (1.48, 1.48, 1.48), without change in Y direction and minimum in X direction and maximum in Z direction (0.8, 0, 1.7); (g) maximum possible rotation in all directions (1.31, 1.31, 1.31), without change in Y direction and maximum in X direction and maximum in Z direction (1.4, 0, 1.55); (h) maximum possible rotation in all directions (0.87, 0.87, 0.87), without change in Z direction and

https://doi.org/10.1017/S0263574714000988 Published online by Cambridge University Press

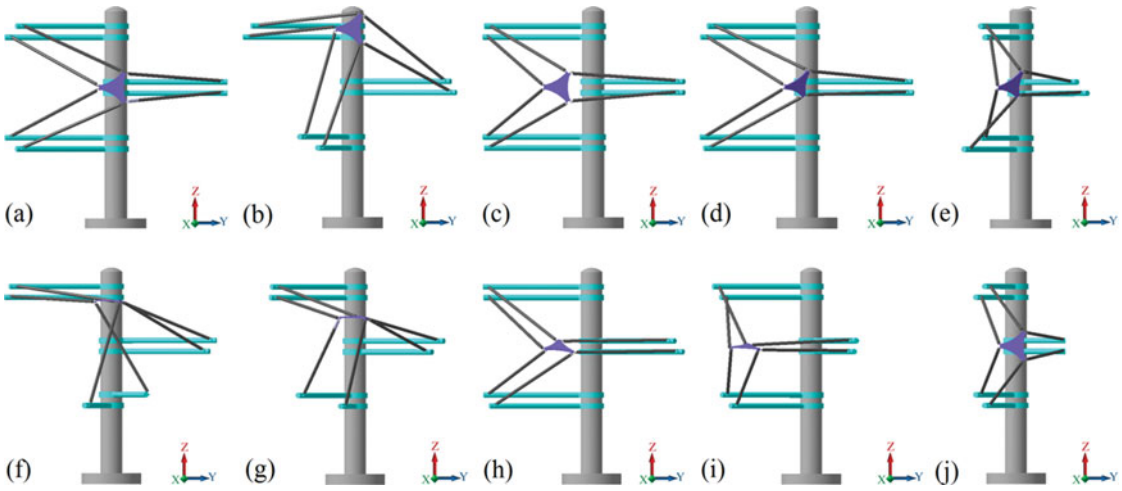

Fig. 16. Different configurations of moving platform within the workspace borders.

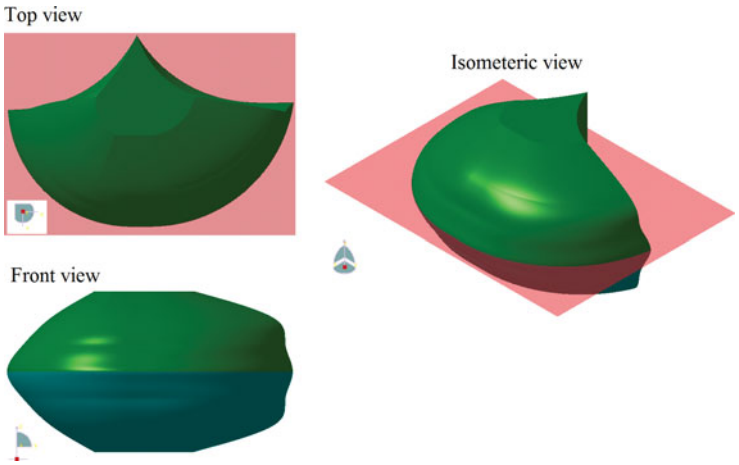

Fig. 17. Three dimensional plot of hexarot workspace, without rotation.

minimum in *XY* plane (0.8, −0.3, 1.275); (i) maximum possible rotation in all directions (1.13, 1.13, 1.13), without change in *Z* direction and maximum in *XY* plane (1.4, −0.6, 1.275); and (j) maximum in *X* direction, open arms (1.8, 0, 1.275) orientation kept unchanged (0, 0, 0).

In order to demonstrate the workspace of the mechanism, a simulation study is performed for a hexarot manipulator. For this purpose, the formulation has been implemented in a programme written in MATLAB for the inverse kinematics and workspace analysis of hexarot mechanism.

This programme has six loops, and examines all points of the mechanism workspace considering the limitations mentioned in section five of this paper. The existence of six loops in the code is due to the existence of six degrees of freedom of the hexarot mechanism. This provides movement in three directions and rotation of platform about the *X*, *Y*, and *Z* axes. By applying the inverse kinematics of position, the written code first calculates angles of rotational joint of all arms. The first applied condition regarding the limitations of workspace is related to arm's length in which by satisfying the length, the code will step into the next loop. In the other case it will get out of the loop and the point will not be considered within workspace of the mechanism. The programme will also consider the next point and investigate the limitations at that point. In the next step, the extreme conditions of the joints and arms collision are examined; moreover, the conditions for singularity which were investigated in Section 5.3 are taken into account. Finally, if all conditions are satisfied then the considered point will be known as a point within the workspace of the manipulator.

Figure 17 shows hexarot workspace which is obtained by transferring cloud of points from MATLAB software to CATIA software. In this case, rotation of platform is neglected and Euler angles conserved in condition of $(0, \pi/2, 0)$.

https://doi.org/10.1017/S0263574714000988 Published online by Cambridge University Press

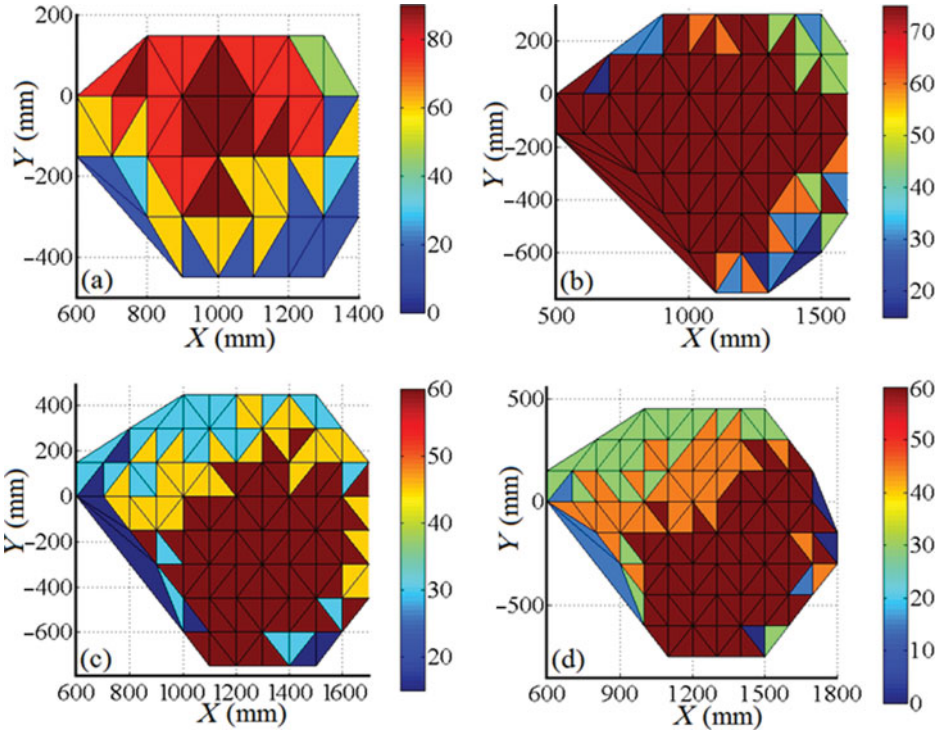

Fig. 18. Reachable positions in the *XY* plane: (a) $Z = 800$ (mm); (b) $Z = 1000$ (mm); (c) $Z = 1200$ (mm); and (d) $Z = 1275$ (mm).

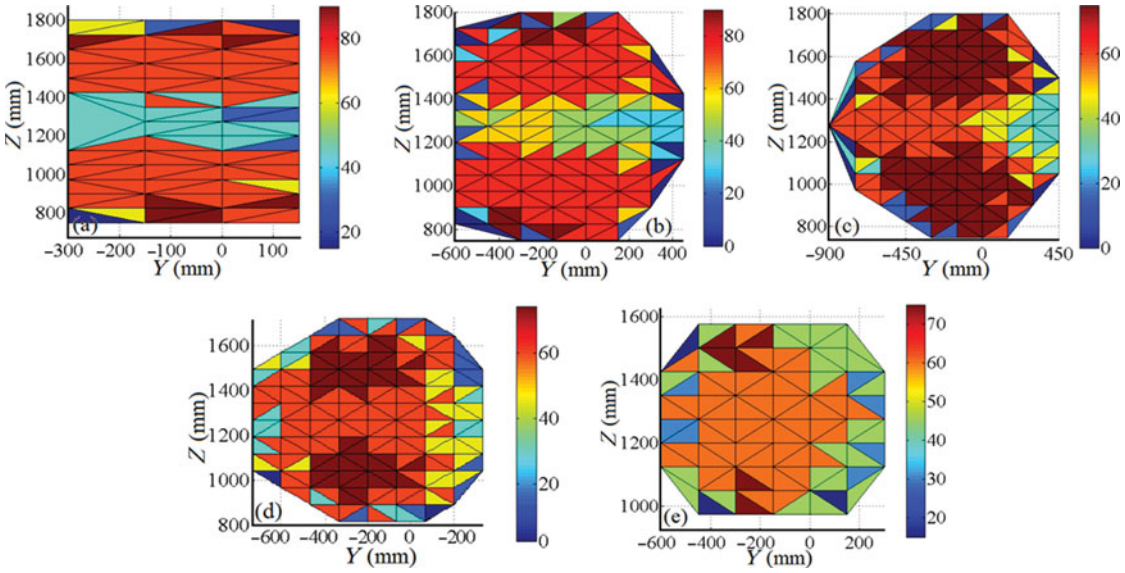

Fig. 19. Reachable positions in the *YZ* plane: (a) $X = 800$ (mm); (b) $X = 1000$ (mm); (c) $X = 1200$ (mm); (d) $X = 1400$ (mm); and (e) $X = 1600$ (mm).

As it is seen in Fig. 17, due to symmetrical placement of arms, the system has a symmetrical plane corresponding to plane $Z = 1.275$ (m). This symmetrical plane is shown in the figure in isometric and top views. Due to rotational limitation in end part of workspace, the primary points of workspace are narrower.

The workspace obtained by analytical method is simulated and illustrated in Figs. 18 and 19 which, respectively, present all reachable positions in the *XY* plane for four different positions in *Z* direction and in *YZ* plane and for five different positions in *X* direction.

https://doi.org/10.1017/S0263574714000988 Published online by Cambridge University Press

In Fig. 18 due to the existence of symmetrical plane of $Z = 1.275$ (m), two areas including workspace with larger Z and workspace with smaller Z are similar. The area of workspace increases from 0.8 (m) to 1.275 (m) when the amount of Z increases and due to similarity this amount decreases on the other side.

In Fig. 19(a), the workspace of manipulator in YZ plane is illustrated in which its X parameter equals to 0.8 (m). This condition includes configurations shown in Figs. 16(b)–16(d), 16(f), and 16(h). Figure 19(d) shows the workspace of hexarot in YZ plane with $X = 1.4$ (m) and includes configurations (i) and (j) of Fig. 16. In Fig. 19(e), the workspace in YZ plane is shown in which its X parameter equals to 1.6 (m) and includes configuration in Fig. 16(e). Configurations (a) and (j) in YZ plane are only points which are not possible to show in these figures.

Regarding Figs. 18 and 19, by increasing the rotation angle in X, Y, and Z directions the size of the workspace is reduced.

7. Conclusions

In this paper, structure of hexarot mechanism and related kinematic relations has been considered. Then all relations of inverse and forward kinematics of position, velocity, and acceleration have been extracted and examined. Since parallel mechanisms have more workspace limitations and complexities compared to serial mechanisms, limitations in joints and arms have been presented in all the points of workspace. Finally, by having all kinematic relations of mechanism and limitations of workspace, the related algorithm for finding the workspace has been developed, and workspace of the mechanism is obtained by programming in MATLAB software.

Appendix 1

The physical specifications of the test manipulator are as follows (all the quantities are given in SI units):

$a_i = 0.961$; $l_i = 1.023$;
$s_1 = 0.308$; $s_2 = 0.0378$;
$h_1 = 0.725$; $h_2 = 0.825$; $h_3 = 1.225$;
$h_4 = 1.325$; $h_5 = 1.725$; $h_6 = 1.825$

Appendix 2

The position and orientation vectors of the moving platform center, i.e., $\mathbf{X} = [\,x\ y\ z\,]^{\mathrm{T}}$ and $\boldsymbol{\theta} = [\,\theta_1\ \theta_2\ \theta_3\,]^{\mathrm{T}}$, are written as functions of time, t, for each path as following:

Path 1:

The moving platform is disoriented and the orientation is kept unchanged during the simulation

$$\mathbf{X} = [\,0.8 + 0.03\mathrm{t} \quad 0.3 + 0.05\mathrm{t} \quad 1.2 + 0.04\mathrm{t}\,]^{\mathrm{T}},$$
$$\boldsymbol{\theta} = [\,\pi \quad \pi/2 \quad 0\,]^{\mathrm{T}}.$$

Path 2:

The moving platform center is moving in a circular path with radius of 0.2 (m) and the orientation of the platform is conserved during the simulation

$$\mathbf{X} = \left[\,1 + 0.2\sin\left(\frac{\pi}{12}t\right) \quad -0.2\cos\left(\frac{\pi}{12}t\right) \quad 1.2\,\right]^{\mathrm{T}},$$
$$\boldsymbol{\theta} = [\,\pi \quad \pi/2 \quad 0\,]^{\mathrm{T}}.$$

Path 3:

The moving platform center is moving with a constant acceleration in a straight line and the orientation of the platform is also changing in positive rolling form at the same time, with a constant

https://doi.org/10.1017/S0263574714000988 Published online by Cambridge University Press

acceleration

$$\mathbf{X} = [\,1 + 0.02t^2 \quad 0 \quad 1.275\,]^{\mathrm{T}},$$
$$\boldsymbol{\theta} = \left[\,\pi \quad \pi/2 \quad \frac{\pi \times t^2}{50}\,\right]^{\mathrm{T}}.$$

Path 4:

The moving platform center remains constant and the orientation of the platform changes in positive yaw form.

$$\mathbf{X} = [\,1 \quad 0 \quad 1.275\,]^{\mathrm{T}},$$
$$\boldsymbol{\theta} = \left[\,\pi + \frac{\pi}{10}t \quad \pi/2 \quad 0\,\right]^{\mathrm{T}}.$$

References

1. K. H. Hunt, "Structural kinematics of in-parallel-actuated robot-arms," *ASME J. Mech. Trans. Autom. Des.* **105**, 705–712 (1983).
2. F. Pierrot, P. Dauchez and A. Fournier, "HEXA: A Fast Six-DOF Fully-Parallel Robot," *Proceedings of the 5th International Conference on Advanced Robotics (ICRA'91)*, Pisa, Italy (1991) pp. 1158–1163.
3. A. Wiegand, M. Hebsacker and M. Honegger, "Parallele Kinematik und Linearmotoren: Hexaglide-ein neues, hochdynamisches Werkzeugmaschinenkonzept," *Technische Rundschau Nr.* **25** (1996).
4. J. P. Lallemand, A. Goudali and S. Zeghloul, "The 6-DOF 2-Delta Parallel Robot," *Robotica* **15**, 407–416 (1997).
5. J. P. Merlet, *Parallel Robots (2 ed.). Solid Mechanics and Its Applications* (**128.** Springer, Dordrecht, the Netherlands, 2006).
6. D. Stewart, "A platform with six degrees of freedom," *Proc. Inst. Mech. Eng.* **180**, 371–386 (1965).
7. M. Isaksson, T. Brogårdh, M. Watson, S. Nahavandi and P. Crothers, "The octahedral hexarot-a novel 6-DOF parallel manipulator", *Mech. Mach. Theory* **55**, 91–102 (2012).
8. C. Reboulet, "Parallel-Structure Manipulator Device for Displacing and Orienting an Object in a Cylindrical Work Space," *U.S. Patent* NO. 5,539,291 (1996).
9. S. Kock, R. Oesterlein and T. Brogårdh, "Industrial Robot," *Patent WO* 03/066289 (2003).
10. M. Merz and S. N. Roy, "Parallel Robot," *U.S. Patent* NO. 7,331,750 (2008).
11. M. Isaksson, T. Brogårdh and S. Nahavandi, "Parallel manipulators with a rotation-symmetric arm system," *ASME J. Mech. Des.* **134**, 114503 (2012).
12. M. Isaksson and M. Watson, "Workspace analysis of a novel six-degrees-of-freedom parallel manipulator with coaxial actuated arms," *ASME J. Mech. Des.* **135**, 1–9 (2013).
13. M. R. Chalak Qazani, S. Pedrammehr, A. Rahmani, M. Shahryari, A. Khani Sheykh Rajab and M. M. Ettefagh, "An experimental study on motion error of hexarot parallel manipulator," *Int. J. Adv. Manuf. Technol.*, (2014) doi: 10.1007/s00170-014-5685-y.
14. K. Harib and K. Srinivasan, "Kinematic and dynamic analysis of Stewart platform-based machine tool structures," *Robotica* **21**, 541–554 (2003).
15. S. Pedrammehr, M. Mahboubkhah and S. Pakzad, "An improved solution to the inverse dynamics of the general Stewart platform," *Proceedings of 2011 IEEE International Conference on Mechatronics ICM 2011*, 5971317 (2011) pp. 392–397.
16. S. Pedrammehr, M. Mahboubkhah and N. Khani, "Improved dynamic equations for the generally configured Stewart platform manipulator," *J. Mech. Sci. Technol.* **26**, 711–721 (2012).
17. S. Pedrammehr, M. Mahboubkhah and N. Khani, "A study on vibration of Stewart platform-based machine tool table," *Int. J. Adv. Manuf. Technol.* **65**, 991–1007 (2013).
18. S. Pedrammehr, M. Mahboubkhah, M. R. Chalak Qazani, A. Rahmani and S. Pakzad, "Forced vibration analysis of milling machine's hexapod table under machining forces," *Stroj. Vestn.-J. Mech. E.* **60**, 158–171 (2014).
19. G. Yang, W. Chen and I.-M. Chen, "A Geometrical Method for the Singularity Analysis of 3-RRRPlanar Parallel Robots with Different Actuation Schemes,"*Proceedings of the 2002 IEEE/RSJ International Conference on Intelligent Robotis and systems*, Lausanne, Switzerland (2002).
20. F. Pierrota1, C. Reynauda1 and A. Fourniera1, "DELTA: A simple and efficient parallel robot," *Robotica* **8**, 105–109 (1990).
21. Y. Li and Q. Xu,"Kinematic analysis of a 3-PRS parallel manipulator,"*Robot. CIM-Int. Manuf.* **23**, 395–408 (2007).

https://doi.org/10.1017/S0263574714000988 Published online by Cambridge University Press

22. J. Xie, W. Qiang, B. Liang and C. Li, "Screw Theory and Singularity Analysis of Parallel Robots," *Proceedings of the 2006 IEEE International Conference on Mechatronics and Automation*, 9097248 (2006) pp. 147–152.
23. D. Oetomo, H. C. Liaw, G. Alici and B. Shirinzadeh, "Direct Kinematics and Analytical Solution to 3RRR Parallel Planar Mechanisms," *IEEE International Conference on Control, Automation, Robotics and Vision*, Singapore (2006) pp. 2251–2256.
24. K. Liu, J. M. Fitzgerald and F. L. Lewis, "Kinematic analysis of a Stewart platform manipulator," *IEEE Trans. Ind. Electron.* **40**, 282–293 (1993).
25. L.-C. Wang and K.-T. Oen, "Numerical direct kinematic analysis of fully parallel linearly actuated platform type manipulators," *Journal of Robotic Systems* **19**, 391–400 (2002).
26. R. Boudreau, "Real time solution to the forward kinematic problem of a general spherical three-degree-of-freedom parallel manipulator," *Proceedings of ASME Design Engineering Technical Conferences* **82**, Boston, MA, USA (1995) pp. 965–971.
27. O. Masory and J. Wang, "Workspace Evaluation of Stewart Platforms," *Proceedings of the ASME 22nd Biennial Mechanisms Conference* **45**, Scottsdale, Arizona (1992) pp. 337–346.
28. E. F. Fichter,"A stewart platform-based manipulator: General theory and practical construction," *Int. J. Robot. Res.* **5**, 157–182 (1986).
29. T. Arai, T. Tanikawa, J. P. Merlet and T. Sendai, "Development of a New Parallel Manipulator with Fixed Linear Actuator," *ASME Japan/USA Symposium on Flexible Automation* **1**, Boston, Massachusetts (1996) pp. 145–149.
30. J. P. Conti, C. M. Clinton, G. Zhang and A. J. Wavering, "Dynamic Variation of the Workspace of an Octahedral Hexapod Machine During Machining," *Technical Research Report*, TR 97–28, ISR (University of Maryland, Maryland, 1997).
31. I. A. Bonev and J. Ryu,"Workspace analysis of 6-PRRS parallel manipulators based on the vertex space concept," *Proceedings of the 1999 ASME Design Engineering Technical Conferences*, Las Vegas, Nevada (Sep. 12–15, 1999).
32. A. Bonev and J. Ryu, "A new approach to orientation workspace analysis of 6-DoF parallel manipulators," *Mech. Mach. Theory* **36**, 15–28 (2001).
33. F. Pernkopf and M. L. Husty, "Workspace Analysis of Stewart-Gough Manipulators Using Orientation Plots," *Proc. MUSME*, 33–38 (2002).
34. T. Huang, J. Wang and D. J. Whitehouse, "Closed Form Solution to Workspace of Hexapod-Based Virtual Axis Machine Tools," *ASME J. Mech. Des.* **121**, 26–31 (1999).
35. C. M. Gosselin, "Determination of the workspace of 6-Dof parallel manipulators," *ASME J. Mech. Des.* **112**, 331–336 (1990).
36. M. Z. A. Majid, Z. Huang and Y. L. Yao, "Workspace analysis of a Six-Degree of freedom, three-prismatic-prismatic-spheric-revolute parallel manipulator," *Int. J. Adv. Manuf. Technol.* **16**, 441–449 (2000).
37. F. Tahmasebi and L. W. Tsai, "Workspace and singularity analysis of a novel Six-DoF parallel minimanipulator," *J. Appl. Mech. Robot.* **1**, 31–40 (1994).
38. C. Zhu, L. Guan, J. Han and L. Wang, "A New Resolution of Workspace Problem of Parallel Machine Tool," *Proceedings ofthe IEEE International Conference on Automation and Logistics Shenyang* (2009) pp. 1002–1007.
39. O. Masory and J. Wang, "Workspace evaluation of stewart platforms," *J. Adv. Rob.* **9**, 443–461 (1995).

https://doi.org/10.1017/S0263574714000988 Published online by Cambridge University Press